Published in final edited form as:
Cell. 2011 June 24; 145(7): 1142–1155. doi:10.1016/j.cell.2011.05.024.

In vivo clonal analysis reveals self-renewing and multipotent adult neural stem cell characteristics

Michael A. Bonaguidi[1,2], **Michael A. Wheeler**[1,*], **Jason S. Shapiro**[1,*], **Ryan P. Stadel**[1,3], **Gerald J. Sun**[1,4], **Guo-li Ming**[1,2,4,#], and **Hongjun Song**[1,2,3,4,#]

[1]Institute for Cell Engineering, Johns Hopkins University School of Medicine, Baltimore, MD 21205, USA

[2]Department of Neurology, Johns Hopkins University School of Medicine, Baltimore, MD 21205, USA

[3]The Human Genetics Pre-doctoral Training Program, Johns Hopkins University School of Medicine, Baltimore, MD 21205, USA

[4]The Solomon H. Snyder Department of Neuroscience, Johns Hopkins University School of Medicine, Baltimore, MD 21205, USA

Summary

Neurogenesis and gliogenesis continue in discrete regions of the adult mammalian brain. A fundamental question remains whether cell genesis occurs from distinct lineage-restricted progenitors or from self-renewing and multipotent neural stem cells in the adult brain. Here, we developed a genetic marking strategy for lineage-tracing of individual, quiescent, and nestin-expressing radial glia-like (RGL) precursors in the adult mouse dentate gyrus. Clonal analysis identified multiple modes of RGL activation, including asymmetric and symmetric self-renewal. Long-term lineage-tracing in vivo revealed a significant percentage of clones that contained RGL(s), neurons, and astrocytes, indicating capacity of individual RGLs for both self-renewal and multi-lineage differentiation. Furthermore, conditional *Pten* deletion in RGLs initially promotes their activation and symmetric self-renewal, but ultimately leads to terminal astrocytic differentiation and depletion in the adult hippocampus. Our study identifies RGLs as self-renewing and multipotent neural stem cells and provides novel insights into in vivo properties of adult neural stem cells.

INTRODUCTION

Stem cells are defined by two characteristic properties, the capacity to renew themselves through mitotic cell division and the capacity to differentiate into specialized cell type(s) (Gage, 2000; Weissman et al., 2001). While capacity for self-renewal and differentiation of various types of stem cells is generally determined based on analysis of a population of

[#]Correspondence should be addressed to: Hongjun Song, Ph.D., Institute for Cell Engineering, Johns Hopkins University School of Medicine, 733 N. Broadway, BRB759, Baltimore, MD 21029, USA, Tel: 443-287-7499; Fax: 410-614-9568, shongju1@jhmi.edu, Guo-li Ming, M.D. & Ph.D., Institute for Cell Engineering, Johns Hopkins University School of Medicine, 733 N. Broadway, BRB779, Baltimore, MD 21029, USA, Tel: 443-287-7498; Fax: 410-614-9568, gming1@jhmi.edu.
[*]These authors contributed equally.

cells, a bona fide stem cell must exhibit both characteristics at the individual cell level. In contrast, lineage-restricted progenitors exhibit limited potential for differentiation and self-renewal. Distinguishing true stem cells from progenitors and understanding basic properties of stem cells at the individual cell level are fundamental goals in stem cell biology and have significant implications for therapeutic application.

Neural stem cells are defined by their ability to self-renew and generate different neural cell types, such as neurons, astrocytes, and oligodendrocytes (Gage, 2000; Temple, 2001). In the developing cortex, neural stem cells first go through symmetric self-renewal to expand the stem cell pool, followed by asymmetric neurogenic cell division to generate neurons, and finally asymmetric gliogenic cell division to produce glia (Gotz and Huttner, 2005; Kriegstein and Alvarez-Buylla, 2009). Elegant time-lapse imaging studies have demonstrated both self-renewal and differentiation of individual neural stem cells in vitro (Davis and Temple, 1994; Noctor et al., 2001). Retroviral labeling also showed that a single retinal progenitor can generate diverse cell types in the postnatal rat retina (Turner and Cepko, 1987). In addition, dye-labeled individual cells in the developing avian neural crest can give rise to multi-lineage clones (Bronner-Fraser and Fraser, 1991). Multipotent neural stem cells have also been proposed to be the source of adult neurogenesis (Gage, 2000; Kriegstein and Alvarez-Buylla, 2009; Ming and Song, 2011). In the subventricular zone (SVZ) of the lateral ventricles, GFAP and nestin expressing radial glia-like precursors produce new interneurons for olfactory bulb and oligodendrocytes for corpus callosum. In the subgranular zone (SGZ) of the dentate gyrus, new granule neurons and astrocytes are continuously generated. The current notion of self-renewing and multipotent adult neural stem cells is largely defined by in vitro evidence that an individual precursor isolated from the adult central nervous system can respond to growth factors to generate neurospheres or monolayer colonies and then can be induced to differentiate into multiple neural lineages upon growth factor withdrawal (Palmer et al., 1999; Reynolds and Weiss, 1992). Studies on cell reprogramming have indicated that lineage-restricted neural progenitors, after exposure to growth factors, can display acquired properties that are not evident in vivo (Gabay et al., 2003; Kondo and Raff, 2000; Palmer et al., 1999). Direct evidence supporting the presence of endogenous adult neural stem cells that are capable of both self-renewal and multi-lineage differentiation at the clonal level in vivo is still missing.

Clonal analysis is particularly important for stem cell biology as cells with precursor properties are not always homogenous (Snippert and Clevers, 2011). In relatively simple systems, such as *Drosophila* and *C. elegans*, stem cells may be individually identified by location and followed by in vivo lineage-tracing (Li and Xie, 2005). As a result, significant mechanistic insight and many basic principles about stem cells have been learned from clonal analyses in these model systems (Doe, 2008; Morrison and Spradling, 2008). In contrast, little is known about clonal properties of stem cells in mammalian systems in vivo. Almost all studies on adult neurogenesis have been carried out at the population level. Nucleotide analog BrdU and onco-retroviruses have been commonly used for lineage-tracing of proliferating neural precursors in the adult brain as a population (Ming and Song, 2005). Since neural stem cells in the adult brain are believed to be largely quiescent (Doetsch et al., 1999; Morshead et al., 1994; Seri et al., 2001), BrdU and retrovirus-based labeling approaches, which require active cell division, are not effective for labeling these cells in vivo. In one previous attempt using retroviruses and lentiviruses to target a small number of $Sox2^+$ neural precursors in the adult SGZ (Suh et al., 2007), no cell clusters were found that indicate both self-renewal and multi-lineage differentiation of labeled neural precursors. The majority of labeled cell clusters contained only a single cell (neuron, astrocyte, or $Sox2^+$ precursor), suggesting a limited capacity for self-renewal. In another study, adenovirus-mediated Cre expression under the control of the GFAP promoter was used to label a patch of radial glia-like cells in the adult SVZ of the Z/EG reporter mice

(Merkle et al., 2007). Along the rostro-caudal axis, these labeled precursors at different locations gave rise to different interneuron subtypes in the adult olfactory bulb, suggesting the presence of a restricted and heterogeneous population of neuronal progenitors. Genetically modified mice with inducible Cre-ER recombination under different promoters have also been used for in vivo fate-mapping of adult neural precursors, but all analyses so far were performed on the population level (Dhaliwal and Lagace, 2011). These early studies therefore leave a critical question unanswered: do endogenous neural stem cells that display both self-renewal and multipotential differentiation at the single cell level exist in the adult mammalian brain? Alternatively, multi-lineage differentiation and self-renewal capacity may represent an emergent property derived from a mixed population of unipotent neural progenitors that are either neurogenic or gliogenic and exhibit limited self-renewal capacity under physiological conditions (Ma et al., 2009).

Significant progress has been made towards understanding mechanisms regulating adult neurogenesis (Ming and Song, 2011). A number of developmental signals, including Wnts, Shh, FGFs, and BMPs, function as extrinsic factors to regulate neural precursors in the adult brain. Several intrinsic factors, such as Sox2, TLX, Pax6, Mash1, NeuroD, Mll1, DISC1, and PTEN, regulate the proliferation of adult neural precursors and their neuronal differentiation in vivo. However, little is known about cellular and molecular mechanisms regulating the behavior of quiescent neural precursors in the adult brain under basal physiological conditions, largely due to a lack of specific approaches to specifically label and manipulate this population. In the current study, we developed a non-invasive, genetic, and sparse labeling approach for the analysis of individual quiescent nestin^{+}GFAP^{+} radial glia-like (RGL) precursors at the clonal level in the adult mouse dentate gyrus. Our study has revealed properties of RGLs as multipotent and self-renewing neural stem cells in the adult brain. We have also identified different modes of RGL self-renewal and novel roles of PTEN in regulating the behavior and capacity of individual RGLs in vivo.

RESULTS

A genetic marking approach for in vivo fate-mapping of individual quiescent nestin^{+} RGLs in the adult mouse hippocampus

Previous studies have shown that multiple neural precursor subtypes express nestin (Figure 1A) and generate new granule neurons in the adult mouse dentate gyrus (Dhaliwal and Lagace, 2011). To examine properties of nestin^{+} neural precursors at the clonal level in the adult brain, we utilized a transgenic approach in mice using the nestin-CreER^{T2} driver for inducible and sparse labeling (Balordi and Fishell, 2007) (Figure S1A). We first screened different reporter lines and identified a combination of nestin-CreER^{T2};Z/EG that did not display any leaky GFP expression in the entire adult dentate gyrus in the absence of tamoxifen injection (n = 8 animals). We next adjusted the dose of tamoxifen to achieve sparse labeling. At the 1X dose (62 mg/kg body weight; single i.p. injection; 2 month-old animals), there were ~ 8 GFP^{+} precursors within the entire SGZ in each dentate gyrus at 2 days post injection (dpi; Figure 1B). We used a set of immunohistological markers and morphological criteria to identify and quantify different cell types labeled with GFP in the dentate gyrus (Figure S1B and Table S1). Over 70% of GFP^{+} precursors in the SGZ exhibited radial glia-like morphology and expressed GFAP and nestin at 2 dpi (Figure 1C; referred to as radial glia-like precursors; RGLs). Importantly, no GFP^{+} RGLs were positive for MCM2, a cell proliferation marker (Maslov et al., 2004) (n = 36 cells/6 animals; Figure 1D), consistent with a quiescent state (Seri et al., 2001). The remaining population of GFP^{+} cells in the SGZ were mostly Tbr2^{+} non radial intermediate progenitor cells (IPCs; Figures 1A and 1C), which were MCM2^{+} (Figure 1D). There were also occasional GFP^{+}S100β^{+} mature astroglia, which were distributed randomly across the whole dentate gyrus (Movie S1). No GFP^{+} astrocytes were MCM2^{+} (n = 23 cells/3 animals at 2 dpi) and extremely few

S100β$^+$ astrocytes were positive for another cell proliferation marker Ki67 in the normal adult dentate gyrus (0.1 ± 0.1%; n = 2960 cells/3 animals), consistent with previous reports that mature astrocytes mostly do not proliferate under basal conditions in the adult hippocampus (Steiner et al., 2004). In contrast, injection of the 4X dose of tamoxifen labeled a large number of precursors in the SGZ at 2 dpi, the majority of which were MCM2$^+$ IPCs (Figures 1B to 1D). In addition, ~20% of GFP$^+$ RGLs were MCM2$^+$ (n = 53 cells/3 animals), whereas GFP$^+$ astrocytes were MCM2$^-$ (n = 169 cells/3 animals at 2 dpi). Thus, the commonly used high doses of tamoxifen preferentially target IPCs and activated RGLs in the dentate gyrus of adult nestin-CreER^{T2} mice.

We next assessed the feasibility of lineage-tracing at the clonal level over the long-term. We reconstructed each individual dentate gyri from serial sections for measurement of distance between labeled cells in 3D space (Movie S1). We set uniform criteria to define an individual GFP$^+$ clone based on distance limits to the clone center (See Experimental Procedures). To obtain a statistical assessment whether a given cell cluster was a clone, we developed a computational model to simulate the cell distribution in the dentate gyrus depending on the observed number of labeled precursors and mature astrocytes under different experimental conditions (Figure S1C). The simulation showed good agreement with the distribution of the measured distance between any GFP$^+$ precursor to the nearest GFP$^+$ cell at 2 dpi after induction with the 1X dose of tamoxifen (Figure 1E). The probability of clonality (P_c) for each cell cluster was then assessed using the simulation-derived standard curves together with distance measurements and the composition of cell types at 1 or 2 month post induction (mpi; Figure 1F). All clusters exhibited greater than 90% probability as clones (Figure 1G). Importantly, this genetic labeling paradigm exhibited small variability in both the number of labeled precursors at 2 dpi and the number of given clones at different time points after induction (Figure S1D). Taken together, these results indicate that the sparse labeling approach yields reproducible in vivo fate-mapping of individual quiescent RGLs with a high confidence of clonality in the adult mouse dentate gyrus.

Multiple modes of self-renewal by RGLs in the adult dentate gyrus

We first quantified the activation rate of GFP$^+$ RGLs in the adult dentate gyrus using the 1X induction paradigm. The percentage of clones that consisted of a single RGL gradually decreased over time from induction (Figure 2A). To characterize RGL activation in detail, we monitored fate choices of individual RGLs directly and unambiguously by focusing on pairs of GFP$^+$ cells that were in the process of cell division, or had just divided and remained in close proximity to one another ($P_c \geq 99.8\%$). As expected, we observed neurogenic asymmetric cell divisions that gave rise to one GFAP$^+$ RGL and one GFAP$^-$ IPC (Figure 2B). We also observed cases of cell clusters consisting of one Sox2$^+$GFAP$^+$ RGL and one or more Sox2$^+$GFAP$^-$ non-radial precursors (Figure S2A), a cell type sometimes regarded as the horizontal precursor (Lugert et al., 2010; Suh et al., 2007). Interestingly, we observed the gliogenic asymmetric cell division that generated one RGL and one GFAP$^+$ bushy astroglia (Figure 2C), suggesting that the glial fate choice can be made at the level of the RGL. On the other hand, no oligogenic asymmetric self-renewal of RGLs was observed (Figures S2B to S2E). After the neurogenic cell division, the RGL returned to quiescence (MCM2$^-$), whereas the IPC entered cell cycle (MCM2$^+$; Figure 2D). In contrast, after the gliogenic cell division, both the RGL and astroglia became quiescent (MCM2$^-$; Figure 2E). Surprisingly, we observed cases of symmetric cell division yielding two RGLs (Figure 2F), which have not been previously reported in the adult brain. Taken together, these results demonstrate at least three modes of RGL self-renewal in the adult dentate gyrus (Figure 2G). Furthermore, RGLs can alternate between active cell cycle and the quiescent state.

Long-term clonal lineage-tracing of RGLs in the adult dentate gyrus

To determine the long-term fate of labeled RGLs, we characterized the composition of individual clones at 1 and 2 mpi using immunohistological and morphological markers (Figure S1B; Figure 3). A total of 54 clones were characterized at 1 mpi using the nestin-CreER^{T2};Z/EG paradigm after induction with 1X tamoxifen. About 83% (45 out of 54) of clones contained at least one RGL (Figure 4A). Among clones with RGL(s), ~69% (31 out of 45) of clones contained at least one RGL and one more cell (Figure 4A), indicating active self-renewal. Among these activated clones, ~6% (2 out of 31) contained multiple RGLs without any other cell types (Figures 3A and 4A), suggesting symmetric self-renewal to expand the RGL pool without differentiation. Importantly, ~13% (4 out of 31) of clones contained the neuronal lineage (e.g. Prox1$^+$), bushy or stellate astrocyte(s) (GFAP$^+$ or S100β$^+$) and at least one RGL (Figures 3B and 4A; Movie S2), indicating both self-renewal and multi-lineage differentiation of a single RGL within the one month period. About 45% (14 out 31) of clones contained at least one RGL and neuronal progeny without any astroglia (Figure 3C), whereas ~35% (11 out of 31) of clones contained at least one RGL and astrocyte(s) without any neuronal progeny (Figure 3D), indicating asymmetric self-renewal and unipotent differentiation. The majority of clones contained less than 6 progeny (Figure 4B), with the three largest clones all containing a large number of IPCs (Figure S4A).

We next characterized the composition of 98 clones at 2 mpi after induction with 1X tamoxifen (Figure 4A). Compared to 1 mpi, there was a significant decrease in the frequency of quiescent clones and an increase in the frequency of clones without RGLs (Figure 4C). The frequencies of clones indicating symmetric or asymmetric self-renewal were similar between 1 and 2 mpi. In particular, the frequency of clones displaying both self-renewal and multipotent differentiation did not significantly change over time. Interestingly, one clone contained three RGLs and two IPCs (Figure 3H; P_c = 97.9%), suggesting three rounds of self-renewal during the two-month period (Figure S3A). Another clone contained two nestin$^+$ RGLs, one Prox1$^+$ neuron with elaborated processes, and one S100β$^+$ astrocyte (Figure 3I; P_c = 97.5%), suggesting that one RGL had gone through three different modes of self-renewal, symmetric, neurogenic and asymmetric, within the two-month period (Figure S3B). Overall, the number of mature progeny in each clone at 1 or 2 mpi was small, with less than 3 neurons or 4 astrocytes (Figures S4B and S4C). No GFP$^+$ clones contained any NG2$^+$ oligodendrocyte progenitors or mature oligodendrocytes, although numerous NG2$^+$ cells were present in the surrounding area (Figures S2B to S2E).

We also characterized some animals at 12 mpi after induction with the 0.5X dose of tamoxifen to reduce the number of induced cells and the probability of clone overlapping (Figures 1B, S4D and S4E). Compared to 2 mpi, there was little decrease in the frequency of quiescent clones, but a dramatic increase in the frequency of clones without RGLs (Figure 4D). Importantly, a significant percentage of clones contained both RGL(s) and differentiated progeny, indicating maintenance of activated RGLs up to one year (Figure 4D).

Taken together, these results demonstrate that a significant percentage of RGLs display properties of both self-renewal and multipotent differentiation within a two-month window in the adult dentate gyrus and at least some activated RGLs were maintained over a 12 month period, therefore identifying RGLs as one type of endogenous multipotent adult neural stem cell.

MADM-based cell lineage-tracing of RGLs in the adult dentate gyrus

To confirm our findings using a different genetic model, we employed the MADM reporter (mosaic-analysis with double markers; Figure S5A) (Zong et al., 2005). In addition to sparse

labeling, the MADM-based approach has the advantage of a two color system: G2-X phase recombination leads to GFP and/or RFP labeling of two daughter cells and all their progeny from a single mitotic event, whereas G1/G0 phase recombination only generates GFP^+RFP^+ clones (Figure 5A). Nestin-$CreER^{T2}$;MADM mice exhibited no leaky GFP or RFP expression in the entire adult dentate gyrus in the absence of tamoxifen injection (n = 5 animals). Within a range between 186 and 373 mg/kg of tamoxifen (single i.p. injection; 2 month-old animals), ~2 precursors were labeled in the SGZ within the entire adult dentate gyrus at 2 dpi, representing a much reduced labeling efficacy in comparison to the Z/EG reporter (Figures 5B and S5B). The majority of labeled precursors in the dentate gyrus were RGLs (75%; n = 15 cells/10 animals). Interestingly, all labeled cells were GFP^+RFP^+ at 2 dpi (Figure 5C), consistent with the notion that they were quiescent at the time of recombination. Thus, the MADM reporter allows for even more stringent clonal analysis of quiescent RGLs in the adult dentate gyrus.

At 2 mpi, distance measurements of labeled progeny to the clone center showed a similar distribution between MADM and Z/EG reporters (Figure S5C), providing an independent validation of our criteria to define clones in this study. Importantly, clone compositions at 2 mpi showed a similar frequency of multipotent and self-renewing clones that contained the neuronal lineage, astrocytes and RGL(s) (Figures 5D and 5E; $P_c \geq 95\%$). All progeny were GFP^+RFP^+ (Figures 5E and S5D). Quantitative analysis further showed that frequencies of different types of clones, including those that were quiescent, symmetrically self-renewed, asymmetrically self-renewed, and differentiated, were similar between Z/EG and MADM reporters (Figure 5F). Together, the convergence of results from two independent reporters validates our clonal analysis approach and provides strong evidence to support RGLs as endogenous self-renewing and multipotent neural stem cells in the adult mouse hippocampus.

Role of PTEN on RGL activation and modes of self-renewal in the adult dentate gyrus

To investigate the molecular mechanism regulating behavior of RGLs, we examined the role of PTEN, a tumor suppressor that regulates several types of somatic stem cells (Hill and Wu, 2009). We generated nestin-$CreER^{T2}$;Z/EG;$Pten^{f/f}$ mice (Figure S6A; PTEN cKO mice) and used the same 1X dose of tamoxifen for induction. As in nestin-$CreER^{T2}$;Z/EG (control) mice, ~73% of labeled cells were RGLs at 2 dpi in adult PTEN cKO mice (n = 5 animals; Figure S6A). Immunostaining of PTEN confirmed its deletion in GFP^+ cells in PTEN cKO mice (Figure S6B).

We next examined the short-term impact of targeted conditional *Pten* deletion in individual RGLs. At 2 dpi, the percentage of clones consisting of a single RGL was dramatically reduced in PTEN cKO mice (Figure 6B). Strikingly, 21% of clones contained RGLs dividing symmetrically, which was not observed in control mice at 2 dpi (Figure 6B). Thus, PTEN functions cell-autonomously within RGLs to maintain quiescence and inhibit symmetric self-renewal of RGLs in the adult dentate gyrus under basal physiological conditions.

Role of PTEN on maintenance and differentiation of RGLs in the adult dentate gyrus

Finally, we examined the long-term consequences of conditional *Pten* deletion in individual RGLs. Assessment of clonality based on distance measurements at 2 dpi and 1 mpi (Figures S6C and S6D) and simulation showed over 90% P_c values (Figure S6E). Compared to control mice at 1 mpi, PTEN cKO mice exhibited decreases in the percentage of quiescent clones consisting of a single RGL and in the percentage of unipotent or multipotent clones (Figures 6C and 6D). This reduction was accompanied by increases in the percentage of clones with multiple RGLs and no differentiated cells (Figures 6A and 6D) and the

percentage of clones with no RGLs in PTEN cKO mice (Figure 6D). Because the increase in the frequency of RGL depletion through differentiation was greater than that of expansion through symmetric self-renewal, *Pten* deletion led to a net reduction of a heterogeneous RGL pool over the one-month period (Figure 6D).

To determine how *Pten* deletion in RGLs impacts their differentiation, we examined the composition of clones without RGLs at 1 mpi in detail. Notably, some GFP^+ cells exhibited morphological features similar to RGLs, such as multiple branches in the granule cell layer, but lacked nestin expression (Figure S6F). These cells may represent a transitional stage of direct differentiation of RGLs into astrocytes (referred to as transition astroglia; TAs), which has been observed during astrocyte differentiation in the developing dentate gyrus in vivo (Brunne et al., 2010). In PTEN cKO mice, there was a dramatic increase in clones containing multiple TAs only and in clones consisting of multiple astrocytes only (Figure S6G). In addition to an increase in glia differentiation, the number of neurons per neurogenic clone was increased in PTEN cKO mice (1.2 ± 0.1 for control; 2.8 ± 0.5 for PTEN cKO). Furthermore, GFP^+ dentate granule neurons without PTEN exhibited increased soma size, ectopic primary dendrites and increased total dendritic length, as previously reported (Figure S6B) (Kim et al., 2009).

Taken together, these results suggest that PTEN exerts multiple functions in RGLs in the adult brain under basal physiological conditions, including maintaining their quiescence and multipotency through inhibition of symmetric self-renewal and astrocytic terminal differentiation.

DISCUSSION

It has been decades since the initial discovery of postnatal mammalian neurogenesis (Altman and Das, 1965) and in vitro derivation of multipotent neural stem cells from adult mouse brains (Reynolds and Weiss, 1992). Yet, a fundamental question in neural stem cell biology has not been hitherto addressed: are multipotent and self-renewing neural stem cells present in the adult mammalian brain? A number of cell types have been proposed to serve as putative neural stem cells in the adult brain, including $GFAP^+$ radial precursors (Doetsch et al., 1999; Seri et al., 2001), $Sox2^+$ non-radial precursors (Suh et al., 2007), and SVZ ependymal cells in response to injury (Carlen et al., 2009). Here we developed a non-invasive, reproducible, and genetic sparse labeling strategy to determine properties of individual $nestin^+GFAP^+$ radial glia-like precursors in vivo. Using two independent reporters, our study demonstrates the existence of self-renewing and multipotent endogenous neural stem cells in the adult mammalian brain (Figure 7A). We also discovered multiple modes of self-renewal and novel functions of PTEN in regulating the behavior and potential of adult neural stem cells in vivo (Figure 7B). These findings have important implications in defining the neural stem cell lineage and understanding their homeostasis in the adult brain.

Clonal approach for in vivo analysis of neural stem cells in the nervous system

Several approaches have previously been attempted for clonal lineage-tracing in mammalian systems (Snippert and Clevers, 2011). The classic retrovirus-based approach (Sanes et al., 1986; Turner and Cepko, 1987) has not yet demonstrated both self-renewal and multi-lineage differentiation from a single precursor in the developing or adult brain in vivo (Morshead et al., 1998; Suh et al., 2007). The MADM-based genetic approach was recently developed for clonally tracing neuronal lineages during development (Zong et al., 2005). Our study represents the initial genetic effort to perform in vivo clonal analysis on neural precursors in the adult brain. This approach may be adapted for clonal analysis of precursors in and outside of the nervous system. This system can be improved with better Cre-driver

lines for more specific targeting of a subtype of precursors and more versatile reporters, such as the Confetti (Snippert et al., 2010) and Brainbow systems (Livet et al., 2007).

Our genetic labeling approach is highly reproducible and provides a high spatial resolution for analysis of individual precursor behavior in vivo with minimal perturbation. Furthermore, this approach targets quiescent RGLs, which have been largely inaccessible due to technical limitations. Some early studies have relied on the BrdU retention approach to identify quiescent precursors, which remains controversial (Snippert and Clevers, 2011). Others have used anti-mitotic treatments to eliminate rapidly proliferating precursors and select for the quiescent population, which does not accurately represent physiological conditions (Doetsch et al., 1999; Seri et al., 2001). Our non-invasive genetic approach has led to several surprising findings. First, the astroglial fate choice of neural precursors appears to be underestimated in the adult mouse dentate gyrus. Previous studies using BrdU and retroviruses suggested that neurogenesis is ten times more frequent than gliogenesis (Steiner et al., 2004). Instead, frequencies of astroglial and neuronal generation were similar in the clonal analysis (Figure 4C). One potential reason for this difference is that neurogenic asymmetric division of an RGL generates an IPC that goes through several rounds of cell division (Figure 2D), whereas gliogenic asymmetric cell division of an RGL generates an astroglia that quickly exits the cell cycle (Figure 2E). Additionally, astrocytes can be generated through direct differentiation of RGLs without cell division (Figures S6F and S6G). Thus, BrdU and retroviral approaches are biased towards labeling IPCs, leading to an underestimation of glial fate choice. Importantly, our study provided direct evidence that the glial fate choice can be made at the level of neural stem cells. Secondly, the amplification capacity of IPCs and neuroblasts appears to be under-appreciated. Instead of an estimated 1 to 2 rounds of cell division by transient amplifying cells (Seri et al., 2001), an individual clone can contain up to 18 IPCs in a tight cluster (Figure 3B; Movie S2), suggesting up to 5 cell cycles. Thirdly, each round of activation of an individual RGL produces a small number of mature neurons and astrocytes under basal conditions. Consistent with a recent finding of significant cell death during the transition from IPCs to neuroblasts in adult hippocampal neurogenesis (Sierra et al., 2010), all large clones observed in this study contained IPCs. These results suggest that the hippocampal circuitry tightly regulates new cell incorporation.

Multipotent and self-renewing neural stem cells in the adult brain

Little is known about basic properties of putative stem cells at the single cell level in mammalian systems in vivo (Snippert and Clevers, 2011). Consistent with previous observations (Lugert et al., 2010; Seri et al., 2001; Suh et al., 2007), nestin^{+}GFAP^{+} RGLs were largely quiescent based upon MCM2 expression and MADM analysis. Once activated, a significant percentage of RGLs display both self-renewal and multipotent differentiation within one month in young adult mice. Some RGLs went through three rounds of cell division and three different modes of self-renewal within a two-month period (Figures 3H and 3I). While many RGLs were depleted over time, importantly, a significant percentage of activated RGLs were maintained over a 12 month period (Figure 4D). In over 300 clones we have examined no labeled cells from the oligodendrocyte lineage were observed, which is not due to the limitation of reporters. A study using Z/EG mice for lineage-tracing has shown that NG2^{+} progenitors give rise to oligodendrocytes, but not new neurons, in the adult dentate gyrus (Kang et al., 2010). Together, these results suggest that neuron/astrocyte and oligodendrocyte lineages are generated from separate pools of precursors in the adult hippocampus under basal physiological conditions.

Our results support the emerging notion of significant heterogeneity in stem cell and progenitor properties, even within the same tissue (Li and Clevers, 2010). Some RGLs exhibited self-renewal and multi-lineage differentiation and a small number were maintained over a long duration. Others exhibited unipotent differentiation and many differentiated over

time without self-renewal. Our result does not fit into a proposed "disposable stem cell model" based on a recent lineage-tracing study at the population level in the adult hippocampus, which suggests that a nestin$^+$ RGL irreversibly exits the quiescent state to rapidly generate multiple neuronal progeny through asymmetric divisions and subsequently convert into a mature astrocyte (Encinas et al., 2011). Our study at the clonal level reveals a much more complex picture and indicates significant heterogeneity in the phenotypic expression of neural stem cell properties in the adult brain. Whether such heterogeneity is due to differences in intrinsic properties of RGLs and/or their local niche remains an interesting question. Our results do not rule out the possibility that other cell types can behave as self-renewing and multipotent neural stem cells in the adult dentate gyrus under basal conditions and/or after stimulation, such as Sox2$^+$ non-radial precursors (Lugert et al., 2010; Suh et al., 2007).

Diverse modes of self-renewal by RGLs in the adult brain

Our study reveals multiple modes of neural stem cell activation in the adult brain and suggests a new model of lineage relationship for neural stem cells in the adult hippocampus (Figure 7A). Activated RGLs face at least four fate choices (Figure 7A). The neuronal lineage begins with an RGL asymmetric cell division to generate a highly proliferative IPC, after which the RGL returns to quiescence. RGLs exhibit a low frequency of symmetric self-renewal, suggesting a surprising capacity of the adult brain to amplify the neural stem cell pool. In addition, there are two independent routes for generating astrocytes in the adult brain: one through asymmetric cell division and the other through direct differentiation via transition astroglia (Brunne et al., 2010). Importantly, an individual RGL has the potential to make all these choices during multiple rounds of self-renewal, as indicated by clones containing multiple RGLs and both neuronal and astroglial lineages (Figure 3I). The total RGL pool therefore reflects a summation of RGL decisions over time: maintenance through quiescence or asymmetric self-renewal, reduction through terminal differentiation, and expansion through symmetric self-renewal.

Our study also revealed unique features of neural stem cells in the adult brain that appear to differ from those in development. Putative neural stem cells in developing brains are continuously proliferating and exhibit temporally segregated symmetric self-renewal, neurogenesis, and gliogenesis in a sequential manner (Temple, 2001). In contrast, adult neural stem cells mostly stay in quiescence, but can be activated to choose from three self-renewal modes and then return to quiescence. Whether these differences are due to intrinsic properties and/or their local niche remains to be investigated.

Multiple roles of PTEN in regulating the behavior and capacity of RGLs

PTEN is a tumor suppresser and a regulator of stem cell behavior in multiple adult somatic tissues (Hill and Wu, 2009). In our study, PTEN loss in quiescent RGLs in the adult SGZ initiates a three-step process (Figure 7B): RGLs are rapidly mobilized into the cell cycle, undergo symmetric cell division and preferentially differentiate into astrocytes. Different from prolonged neurogenesis observed after PTEN removal in proliferating adult SVZ cultures (Gregorian et al., 2009), PTEN deletion in RGLs reduced rather than expanded the overall RGL pool in the adult hippocampus within a one month period. Interestingly, loss of PTEN in hematopoietic stem cells also leads to loss of quiescence and subsequent exhaustion in vivo (Yilmaz et al., 2006; Zhang et al., 2006). Previous studies have shown that PTEN loss driven by the mGFAP-Cre promoter during late embryonic development increases cell proliferation and neuroblast number in the young adult SVZ (Gregorian et al., 2009). It is unclear whether these GFAP$^+$ cells in the SVZ are precursors or niche astrocytes. As an alternative hypothesis, PTEN may play different roles among various neural cell types. Indeed, we observed that PTEN deletion differentially promoted neuron survival in

the adult hippocampus while abolishing multipotency of RGLs analyzed at 1 mpi. Furthermore, RGLs may be heterogeneous in their response to PTEN deletion. In contrast to the overall decrease in the RGL pool, some RGLs underwent symmetric self-renewal. Together, these findings underscore the necessity to study stem cell function at the single cell level and indicate that PTEN is a critical component in the maintenance of neural stem cell capacity.

In summary, we have developed a genetic labeling approach for clonal analysis of quiescent neural stem cells in vivo. Our identification of self-renewing and multipotent endogenous neural stem cells supports a new lineage model in the adult hippocampus. Our findings provide a number of novel insights into potential targets for intervention to enhance adult neurogenesis during aging and in degenerative neurological disorders. The presence of RGL symmetric cell division allows for possibilities to amplify the neural stem cell pool in the adult brain. Given the relatively small clone sizes, increasing the proliferation of IPCs and survival of neuronal progeny could be an important strategy to enhance neurogenesis. Furthermore, preventing aberrant loss of PTEN signaling may offer a means of guarding against depletion of the adult neural stem cell pool during aging.

EXPERIMENTAL PROCEDURES

Animals and Tamoxifen Administration

All mice used in the study were back-crossed to the C57BL/6 background to ensure the reproducibility of clonal induction with specific doses of tamoxifen. Animals were housed in a 14 hr light/10 hr dark cycle with free access to food. All animal procedures were in accordance with institutional guidelines. A stock of tamoxifen (62 mg/ml; Sigma; T5648) was prepared in a 5:1 ratio of corn oil to ethanol at 37°C with occasional vortexing. A single tamoxifen or vehicle dose was i.p. injected into 8–10 week-old mice at various concentrations: 31 – 248 mg/kg for the Z/EG reporter and 186 – 373 mg/kg for the MADM reporter.

Immunostaining, Confocal Imaging and Processing

Coronal brain sections (45 μm in thickness) through the entire dentate gyrus were maintained in the serial order and immunostaining was performed as described (Ge et al., 2006). Antibodies used in this study are listed in Table S1. Confocal images were used to confirm GFP^+ cell identity according to immunohistological and morphological properties (Figure S1B). For 3D reconstruction, optical stacks from the entire dentate gyrus were serially aligned using Reconstruct 1.1.0 (John C. Fiala, the National Institutes of Health). These images were refined using an in-house MATLAB script (The MathWorks, Inc.).

Clonal Analysis

Analyzed dentate volume included the molecular layer, stratum granulosum (granule cell layer), SGZ and hilus, but excluded the polymorphic layer (CA4) protruding into the posterior dentate gyrus. Serial sections were first screened for candidate clones, which were defined as possessing at least (1) an RGL, (2) neuronal cell(s) in close spatial proximity, or (3) astroglia in close spatial proximity to other astroglia or neuronal cells. Distance measurements were performed in Imaris (Bitplane) and an in-house MATLAB script was used to determine the distances among every spot. A ring with a radius of 150 μm from the clone center was used to determine the clone composition for 1 and 2 mpi analysis. Clones were categorized according to the presence or absence of an RGL and the type of progeny (Figures 3 and 4). A computational simulation was used for statistical assessment of the probability of whether each cell cluster was a clone. Precursors and astroglia were randomly placed in a model dentate gyrus for distance measurements in MATLAB and this procedure

was repeated 5000 times to generate a distribution of distance measurements (Figures 1E and S6C, red lines) and reverse cumulative distribution plots (Figure S1C). Each putative clone was assigned a probability as a clone (P_c) equal to 1 minus the probability that two cells could have been induced at 2 dpi within the clone's radius of each other (x 100%).

Supplementary Material

Refer to Web version on PubMed Central for supplementary material.

Acknowledgments

We thank D. Lee, and members of Song and Ming laboratories for discussion, G. Fishell for sharing nestin-CreER^{T2} mice, L. DeBiase for NG2 antibodies, J. Song, S. Danzer, C. Song,Y. Namgung, X. Duan and K. Sailor for help, and Q. Hussaini, Y. Cai and L. Liu for technical support. This work was supported by grants from NIH (NS047344, AG024984) and NARSAD to H.S., from NIH (NS048271, HD069184) and MSCRF to G.L.M. M.A.B. was a MSCRF fellow.

REFERENCE

Altman J, Das GD. Post-natal origin of microneurones in the rat brain. Nature. 1965; 207:953–956. [PubMed: 5886931]

Balordi F, Fishell G. Mosaic removal of hedgehog signaling in the adult SVZ reveals hat the residual wild-type stem cells have a limited capacity for self-renewal. J Neurosci. 2007; 27:14248–14259. [PubMed: 18160632]

Bronner-Fraser M, Fraser SE. Cell lineage analysis of the avian neural crest. Development. 1991 Suppl 2:17–22. [PubMed: 1726831]

Brunne B, Zhao S, Derouiche A, Herz J, May P, Frotscher M, Bock HH. Origin, maturation, and astroglial transformation of secondary radial glial cells in the developing dentate gyrus. Glia. 2010; 58:1553–1569. [PubMed: 20549747]

Carlen M, Meletis K, Goritz C, Darsalia V, Evergren E, Tanigaki K, Amendola M, Barnabe-Heider F, Yeung MS, Naldini L, et al. Forebrain ependymal cells are Notch-dependent and generate neuroblasts and astrocytes after stroke. Nat Neurosci. 2009; 12:259–267. [PubMed: 19234458]

Davis AA, Temple S. A self-renewing multipotential stem cell in embryonic rat cerebral cortex. Nature. 1994; 372:263–266. [PubMed: 7969470]

Dhaliwal J, Lagace DC. Visualization and genetic manipulation of adult neurogenesis using transgenic mice. Eur J Neurosci. 2011; 33:1025–1036. [PubMed: 21395845]

Doe CQ. Neural stem cells: balancing self-renewal with differentiation. Development. 2008; 135:1575–1587. [PubMed: 18356248]

Doetsch F, Caille I, Lim DA, Garcia-Verdugo JM, Alvarez-Buylla A. Subventricular zone astrocytes are neural stem cells in the adult mammalian brain. Cell. 1999; 97:703–716. [PubMed: 10380923]

Encinas JM, Michurina TV, Peunova N, Park JH, Tordo J, Peterson DA, Fishell G, Koulakov A, Enikolopov G. Division-coupled astrocytic differentiation and age-related depletion of neural stem cells in the adult hippocampus. Cell Stem Cell. 2011; 8:566–579. [PubMed: 21549330]

Gabay L, Lowell S, Rubin LL, Anderson DJ. Deregulation of dorsoventral patterning by FGF confers trilineage differentiation capacity on CNS stem cells in vitro. Neuron. 2003; 40:485–499. [PubMed: 14642274]

Gage FH. Mammalian neural stem cells. Science. 2000; 287:1433–1438. [PubMed: 10688783]

Ge S, Goh EL, Sailor KA, Kitabatake Y, Ming GL, Song H. GABA regulates synaptic integration of newly generated neurons in the adult brain. Nature. 2006; 439:589–593. [PubMed: 16341203]

Gotz M, Huttner WB. The cell biology of neurogenesis. Nat Rev Mol Cell Biol. 2005; 6:777–788. [PubMed: 16314867]

Gregorian C, Nakashima J, Le Belle J, Ohab J, Kim R, Liu A, Smith KB, Groszer M, Garcia AD, Sofroniew MV, et al. Pten deletion in adult neural stem/progenitor cells enhances constitutive neurogenesis. J Neurosci. 2009; 29:1874–1886. [PubMed: 19211894]

Hill R, Wu H. PTEN, stem cells, and cancer stem cells. J Biol Chem. 2009; 284:11755–11759. [PubMed: 19117948]

Kang SH, Fukaya M, Yang JK, Rothstein JD, Bergles DE. NG2(+) CNS Glial Progenitors Remain Committed to the Oligodendrocyte Lineage in Postnatal Life and following Neurodegeneration. Neuron. 2010; 68:668–681. [PubMed: 21092857]

Kim JY, Duan X, Liu CY, Jang MH, Guo JU, Pow-anpongkul N, Kang E, Song H, Ming GL. DISC1 regulates new neuron development in the adult brain via modulation of AKT-mTOR signaling through KIAA1212. Neuron. 2009; 63:761–773. [PubMed: 19778506]

Kondo T, Raff M. Oligodendrocyte precursor cells reprogrammed to become multipotential CNS stem cells. Science. 2000; 289:1754–1757. [PubMed: 10976069]

Kriegstein A, Alvarez-Buylla A. The glial nature of embryonic and adult neural stem cells. Annu Rev Neurosci. 2009; 32:149–184. [PubMed: 19555289]

Li L, Clevers H. Coexistence of quiescent and active adult stem cells in mammals. Science. 2010; 327:542–545. [PubMed: 20110496]

Li L, Xie T. Stem cell niche: structure and function. Annu Rev Cell Dev Biol. 2005; 21:605–631. [PubMed: 16212509]

Livet J, Weissman TA, Kang H, Draft RW, Lu J, Bennis RA, Sanes JR, Lichtman JW. Transgenic strategies for combinatorial expression of fluorescent proteins in the nervous system. Nature. 2007; 450:56–62. [PubMed: 17972876]

Lugert S, Basak O, Knuckles P, Haussler U, Fabel K, Gotz M, Haas CA, Kempermann G, Taylor V, Giachino C. Quiescent and active hippocampal neural stem cells with distinct morphologies respond selectively to physiological and pathological stimuli and aging. Cell Stem Cell. 2010; 6:445–456. [PubMed: 20452319]

Ma DK, Bonaguidi MA, Ming GL, Song H. Adult neural stem cells in the mammalian central nervous system. Cell Res. 2009; 19:672–682. [PubMed: 19436263]

Maslov AY, Barone TA, Plunkett RJ, Pruitt SC. Neural stem cell detection, characterization, and age-related changes in the subventricular zone of mice. J Neurosci. 2004; 24:1726–1733. [PubMed: 14973255]

Merkle FT, Mirzadeh Z, Alvarez-Buylla A. Mosaic organization of neural stem cells in the adult brain. Science. 2007; 317:381–384. [PubMed: 17615304]

Ming, G-l; Song, H-j. Adult Neurogenesis in the Mammalian Brain: Significant Answers and Significant Questions. Neuron. 2011 In press.

Ming GL, Song H. Adult neurogenesis in the mammalian central nervous system. Annu Rev Neurosci. 2005; 28:223–250. [PubMed: 16022595]

Morrison SJ, Spradling AC. Stem cells and niches: mechanisms that promote stem cell maintenance throughout life. Cell. 2008; 132:598–611. [PubMed: 18295578]

Morshead CM, Craig CG, van der Kooy D. In vivo clonal analyses reveal the properties of endogenous neural stem cell proliferation in the adult mammalian forebrain. Development. 1998; 125:2251–2261. [PubMed: 9584124]

Morshead CM, Reynolds BA, Craig CG, McBurney MW, Staines WA, Morassutti D, Weiss S, van der Kooy D. Neural stem cells in the adult mammalian forebrain: a relatively quiescent subpopulation of subependymal cells. Neuron. 1994; 13:1071–1082. [PubMed: 7946346]

Noctor SC, Flint AC, Weissman TA, Dammerman RS, Kriegstein AR. Neurons derived from radial glial cells establish radial units in neocortex. Nature. 2001; 409:714–720. [PubMed: 11217860]

Palmer TD, Markakis EA, Willhoite AR, Safar F, Gage FH. Fibroblast growth factor-2 activates a latent neurogenic program in neural stem cells from diverse regions of the adult CNS. J Neurosci. 1999; 19:8487–8497. [PubMed: 10493749]

Reynolds BA, Weiss S. Generation of neurons and astrocytes from isolated cells of the adult mammalian central nervous system. Science. 1992; 255:1707–1710. [PubMed: 1553558]

Sanes JR, Rubenstein JL, Nicolas JF. Use of a recombinant retrovirus to study post-implantation cell lineage in mouse embryos. Embo J. 1986; 5:3133–3142. [PubMed: 3102226]

Seri B, Garcia-Verdugo JM, McEwen BS, Alvarez-Buylla A. Astrocytes give rise to new neurons in the adult mammalian hippocampus. J Neurosci. 2001; 21:7153–7160. [PubMed: 11549726]

Sierra A, Encinas JM, Deudero JJ, Chancey JH, Enikolopov G, Overstreet-Wadiche LS, Tsirka SE, Maletic-Savatic M. Microglia shape adult hippocampal neurogenesis through apoptosis-coupled phagocytosis. Cell Stem Cell. 2010; 7:483–495. [PubMed: 20887954]

Snippert HJ, Clevers H. Tracking adult stem cells. EMBO Rep. 2011; 12:113–122. [PubMed: 21252944]

Snippert HJ, van der Flier LG, Sato T, van Es JH, van den Born M, Kroon-Veenboer C, Barker N, Klein AM, van Rheenen J, Simons BD, Clevers H. Intestinal crypt homeostasis results from neutral competition between symmetrically dividing Lgr5 stem cells. Cell. 2010; 143:134–144. [PubMed: 20887898]

Steiner B, Kronenberg G, Jessberger S, Brandt MD, Reuter K, Kempermann G. Differential regulation of gliogenesis in the context of adult hippocampal neurogenesis in mice. Glia. 2004; 46:41–52. [PubMed: 14999812]

Suh H, Consiglio A, Ray J, Sawai T, D'Amour KA, Gage FH. In vivo fate analysis reveals the multipotent and self-renewal capacities of Sox2+ neural stem cells in the adult hippocampus. Cell Stem Cell. 2007; 1:515–528. [PubMed: 18371391]

Temple S. The development of neural stem cells. Nature. 2001; 414:112–117. [PubMed: 11689956]

Turner DL, Cepko CL. A common progenitor for neurons and glia persists in rat retina late in development. Nature. 1987; 328:131–136. [PubMed: 3600789]

Weissman IL, Anderson DJ, Gage FH. Stem and progenitor cells: origins, phenotypes, lineage commitments, and transdifferentiations. Annu Rev Cell Dev Biol. 2001; 17:387–403. [PubMed: 11687494]

Yilmaz OH, Valdez R, Theisen BK, Guo W, Ferguson DO, Wu H, Morrison SJ. Pten dependence distinguishes haematopoietic stem cells from leukaemia-initiating cells. Nature. 2006; 441:475–482. [PubMed: 16598206]

Zhang J, Grindley JC, Yin T, Jayasinghe S, He XC, Ross JT, Haug JS, Rupp D, Porter-Westpfahl KS, Wiedemann LM, et al. PTEN maintains haematopoietic stem cells and acts in lineage choice and leukaemia prevention. Nature. 2006; 441:518–522. [PubMed: 16633340]

Zong H, Espinosa JS, Su HH, Muzumdar MD, Luo L. Mosaic analysis with double markers in mice. Cell. 2005; 121:479–492. [PubMed: 15882628]

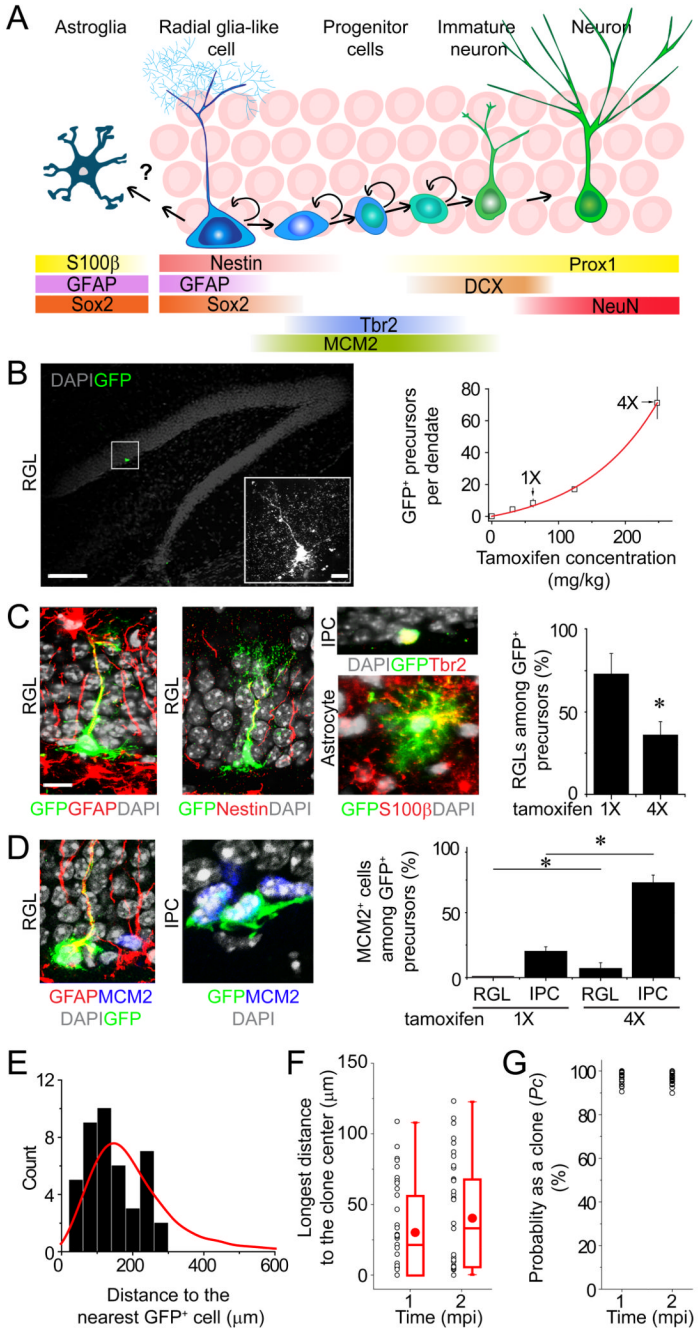

Figure 1. A genetic marking strategy for in vivo analysis of individual nestin^{+} radial glia-like neural precursors in the adult mouse dentate gyrus

(A) A schematic diagram indicating the current view of lineage relationships and marker expression during adult hippocampal neurogenesis.

(B) Tamoxifen dose responses on the number of labeled precursors in the dentate gyrus of adult nestin-CreER^{T2};Z/EG mice. Shown is a sample projected confocal image of GFP and DAPI. Scale bar: 100 μm (10 μm for the insert). Also shown is a summary of the number of GFP^{+} precursors in each dentate gyrus. Values represent mean ± SD (n = 5–12 dentate gyri).

(C and D) Characteristics of labeled cells 2 days after induction with 1X or 4X dose of tamoxifen. In (C), shown are sample confocal images of immunostaining of GFP, GFAP or

nestin (for RGL), Tbr2 (for IPC), and S100β (for mature astrocyte), and a summary of the percentage of GFP^+ cells with RGL characteristics among all labeled precursors within the adult subgranular zone. Values represent mean ± SEM (n = 5; *: $P < 0.05$; Student's t-test). In (D), shown are sample confocal images of immunostaining of MCM2 and the percentage of GFP^+ precursor subtypes that were $MCM2^+$. Value represent mean ± SEM (n = 3; *: $P < 0.05$; Student's t-test). Scale bars: 10 μm.

(E to G) Quantitative analysis of clonality at 1 and 2 mpi after induction with the 1X dose of tamoxifen. Shown in (E) is the distribution of measured distances between a GFP^+ precursor and its nearest GFP^+ cell in the dentate gyrus at 2 dpi (histogram) and data from a computer simulated distribution of distances (8 precursors and 14 astroglia; red line). Shown in (F) is a summary of measured longest distance of a GFP^+ cell to the clone center at 1 and 2 mpi. Each dot represents data from one clone. Also shown are box-plots (middle dot represents mean; middle line represents median; box represents 25^{th} to 75^{th} percentile; whiskers are minimum and maximum values). Shown in (G) is the calculated probability as a clone (P_c) for each cell cluster based on distance measurements in (F) and standard curves in Figure S1C.

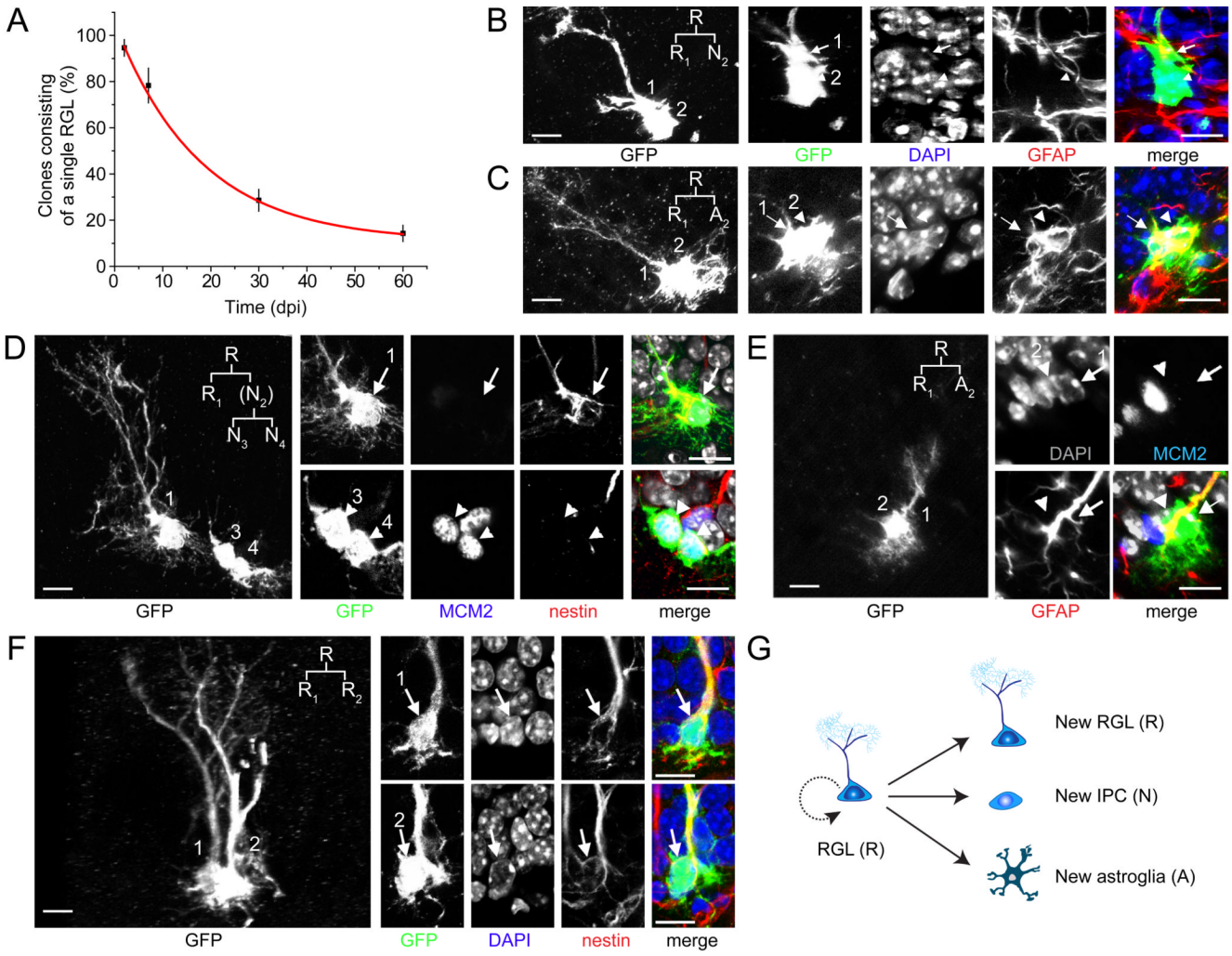

Figure 2. Different modes of self-renewal by individual RGLs in the adult dentate gyrus

(A) Time course of activation of labeled RGLs in the adult dentate gyrus after induction with the 1X dose of tamoxifen. Shown is the quantification of clones consisting of a single RGL, indicating quiescence. Values present mean ± SEM (n = 3–8 animals).

(B–F) Sample confocal images of GFP^+ cells in the process of, or right after RGL cell division ($P_c \geq 99.8\%$). Shown are samples of neurogenic asymmetric cell division (B, D), astrogenic asymmetric cell division (C, E) and symmetric cell division (F). The potential lineage relationship is indicated in the insert. R: RGL; N: neuronal lineage; A: astroglia. Note that after cell division, the RGL and newborn astroglia returned to quiescence ($MCM2^-$; D, E), whereas the IPC re-entered the cell cycle ($MCM2^+$; D). Scale bars: 10 μm.

(G) A schematic diagram of three modes of self-renewal made by an RGL in the adult dentate gyrus.

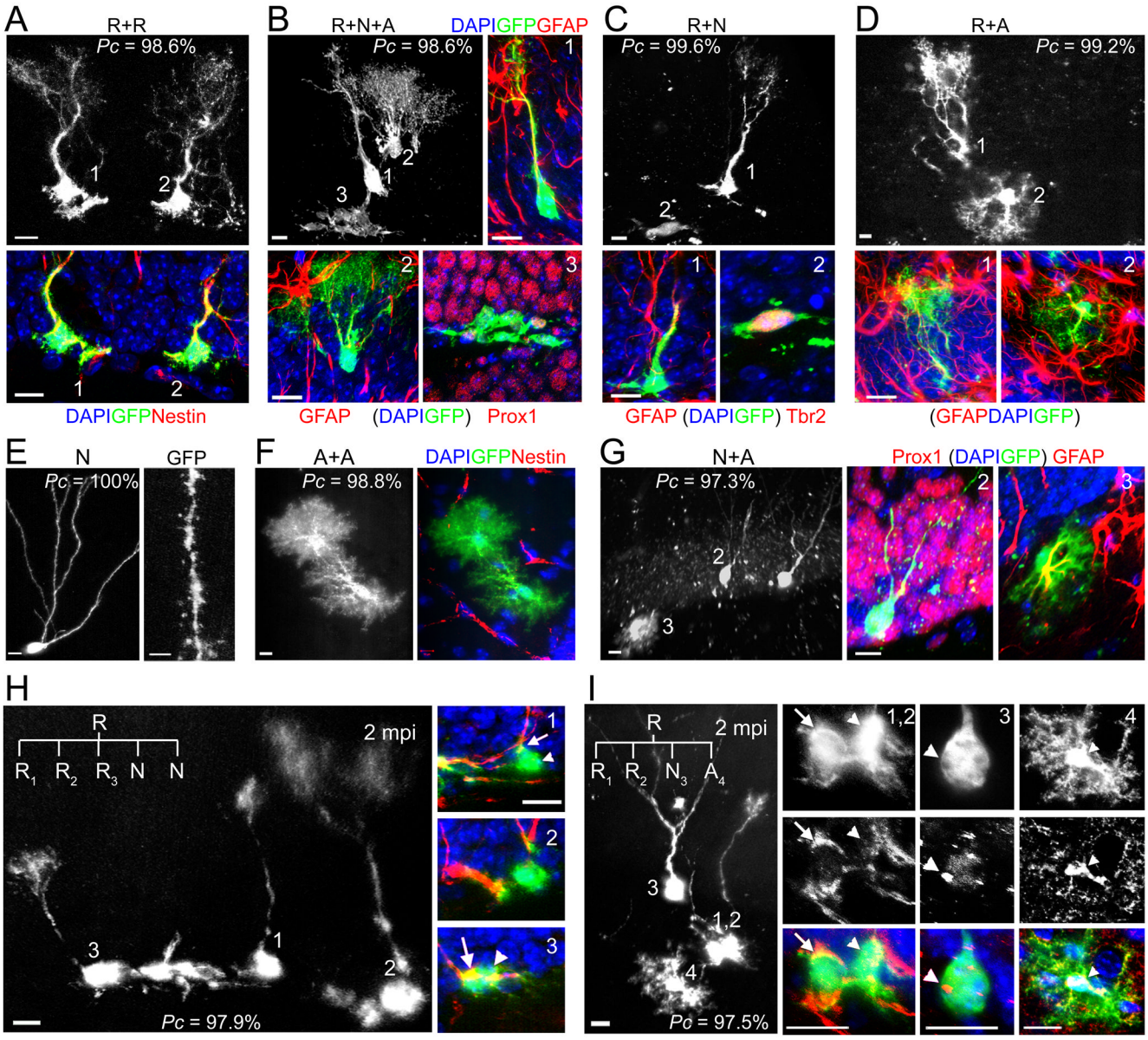

Figure 3. Clone classifications after long-term lineage-tracing of individual RGLs in the adult dentate gyrus

(A–D) Sample confocal images of clones with active self-renewal. The clone in (A) consisted of two nestin$^+$ RGLs, but no other cells, indicating symmetric self-renewal and an expansion of the RGL pool. The clone in (B) consisted of a GFAP$^+$ RGL (1), a GFAP$^+$ bushy astrocyte (2) and a cluster of 18 cells of the neuronal lineage (3), some of which expressed dentate granule cell marker Prox1, indicating self-renewal and multi-lineage differentiation (See 3D reconstruction in Movie S2). The clone in (C) consisted of a GFAP$^+$ RGL (1) and Tbr2$^+$ IPCs (2), indicating self-renewal and unipotential neurogenic differentiation. The clone in (D) consisted of a GFAP$^+$ RGL (1) and a GFAP$^+$ bushy astrocyte (2), indicating self-renewal and unipotential astrogenic differentiation. The P_c value for each clone is also shown. Scale bars: 10 μm.

(E–G) Sample confocal images of differentiated clones without an RGL. The clone in (E) consisted of a mature neuron with prominent dendritic spines (Scale bar: 2 μm). The clone

in (F) consisted of two nestin^{-} bushy astrocytes. The clone in (G) consisted of two Prox1^{+} neurons (2) and one GFAP^{+} stellate astrocyte (3). Scale bars: 10 μm.

(H) Sample confocal images of a clone indicating multiple rounds of self-renewal within two months. The clone consists of three nestin^{+} RGLs (1, 2, 3) and two IPCs. Scale bars: 10 μm. The potential lineage relationship is illustrated in Figure S3A.

(I) Sample confocal images of a clone indicating multiple modes of self-renewal and multi-lineage differentiation within the two month period, including symmetric, neurogenic asymmetric and astrogliogenic asymmetric self-renewal. The clone consisted of two nestin^{+} RGLs (1, 2), one Prox1^{+} mature neuron with elaborate dendritic arborization (3), and one S100β^{+} stellate astrocyte (4). Scale bars: 10 μm. The potential lineage relationship is illustrated in Figure S3B.

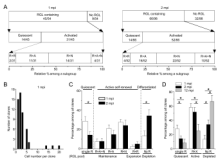

Figure 4. Summary of clone properties at different time points after labeling

(A) Quantification of the frequency of different types of clones at 1 and 2 mpi after induction with 1X dose of tamoxifen. Data represent the relative frequency among a defined subgroup of clone categories. The number of a specific type and total number of clones within a subgroup are indicated in parenthesis. R:RGL; A: astroglia; N: neuronal lineage.

(B) A histogram of the number of progeny within each clone at 1 mpi.

(C) Quantitative comparison of the frequency of different clone compositions observed at 1 and 2 mpi. The frequency of each type among all clones per dentate gyrus is plotted for comparison using the same dataset as in (A). R: RGL; A: astroglia; N: neuronal lineage. Values represent mean ± SEM (*: $P < 0.05$; student's t-test; n = 7 and 13 dentate gyri for 1 and 2 mpi, respectively).

(D) Quantitative comparison of the frequency of clones with quiescent (single R), clones with activated RGLs (R+X), and clones depleted of RGLs (No R) at 1, 2 and 12 mpi. The same dataset as in (A) is used for 1 and 2 mpi. For 12 mpi, animals were induced with 0.5X dose of tamoxifen (n = 7 dentate gyri). Values represent mean ± SEM (*: $P < 0.05$; student's t-test).

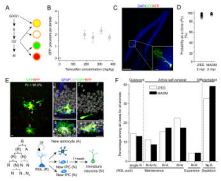

Figure 5. MADM-based analysis of nestin^{+} radial glia-like neural precursors in the adult brain

(A) A schematic diagram indicating potential color combinations from the MADM-based reporter depending on the timing of the Cre-mediated recombination. G2-X phase recombination leads to two color labeling of two daughter cells and all their progeny from a single mitotic event, whereas G1/G0 phase recombination only generates GFP^{+}RFP^{+} (yellow) clones.

(B) Tamoxifen dose responses on the number of labeled precursors in the dentate gyrus of adult nestin-CreER^{T2};MADM mice at 2 dpi. Values represent mean ± SD (n = 3 dentate gyri).

(C) Sample projection confocal images of a single RGL labeled with both GFP and RFP in the adult dentate gyrus. Scale bars: 100 μm (10 μm for the insert).

(D) A summary of probability as a clone (P_c) for all labeled cell clusters in the MADM study. The probability was calculated based on the computational simulation (in Figure S1C) and direct distance measurement of the longest distance from progeny to the clone center (Figure S5C).

(E) Sample confocal images of a clone indicating self-renewal and multi-lineage differentiation within the two month window. Shown are confocal images of a clone consisting of a GFAP^{+} RGL (1), an immature neuron (2), a GFAP^{+} bushy astrocyte (3), and a cluster of IPCs (4), and diagrams of the potential lineage relationship. Scale bars: 10 μm.

(F) Comparison of the frequency of clone compositions observed at 2 mpi between Z/EG (n = 98 clones; same as in Figure 4A) and MADM reporters (n = 23 clones). The frequency of each type among clones from all animals is plotted. R: RGL; A: astroglia; N: neuronal lineage.

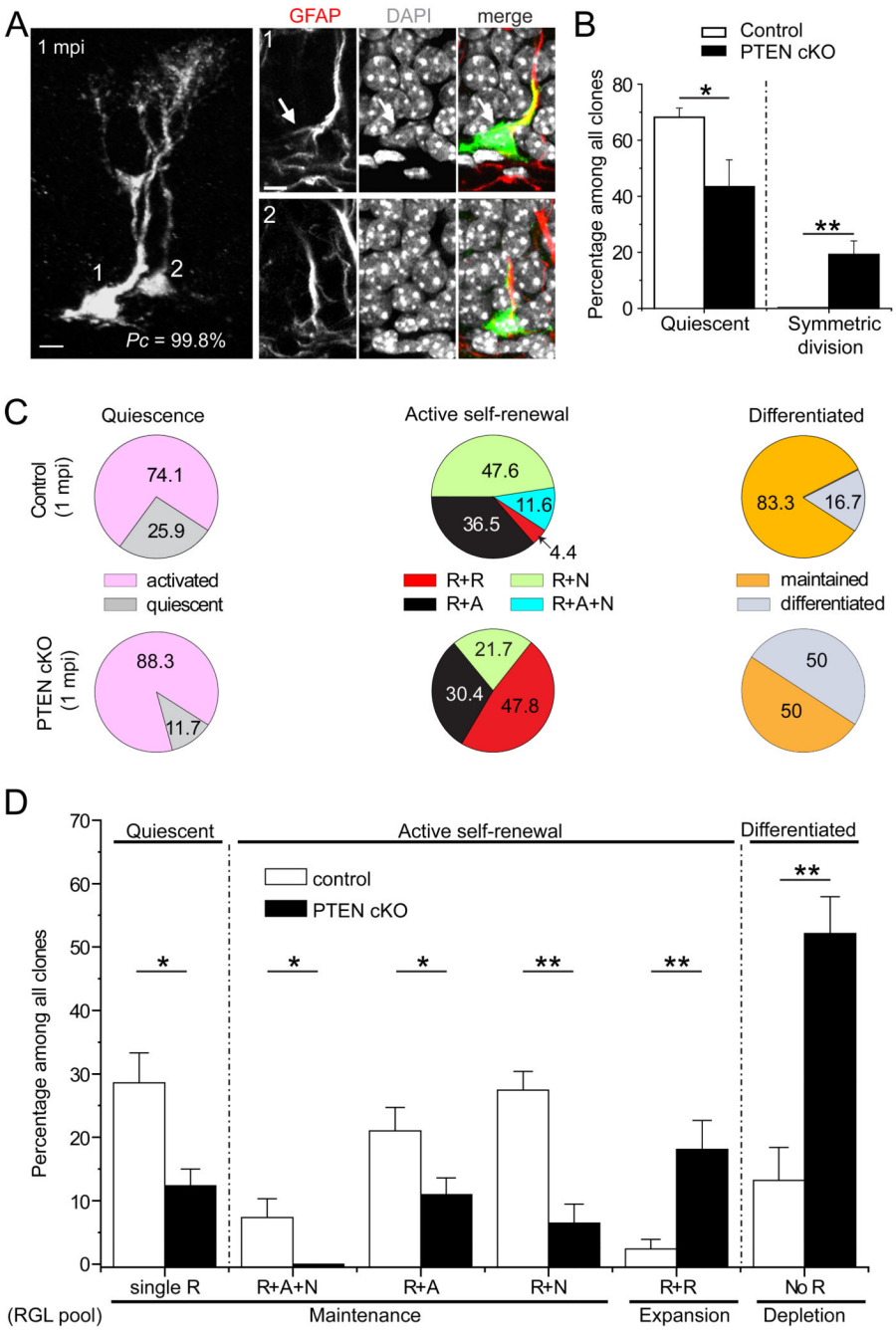

Figure 6. Roles of PTEN in regulating quiescence, self-renewal modes and differentiation of RGLs in the adult dentate gyrus

(A) Sample confocal images of a clone consisting of two RGLs with *Pten* deletion at 1 mpi. Scale bars: 10 μm.

(B) Rapid activation and symmetric self-renewal of RGLs after *Pten* deletion in individual RGLs. Shown is the quantification of quiescence and symmetric self-renewal of RGLs in control (n = 6) and PTEN cKO mice (n = 5) at 2 dpi. Values represent mean ± SEM (**: $P < 0.01$; *: $P < 0.05$; student's t-test).

(C and D) Quantitative comparison of the frequency of different clone types between control (n = 7) and PTEN cKO (n = 6) at 1 mpi. Shown are pie charts of the relative frequency

among each category (C) and the summary of the frequency of different types among all clones (D). The detailed analysis of differentiated clones is shown in Figure S6G. R: RGL, A: astroglia, N: neuronal lineage. Values represent mean ± SEM (**: $P < 0.01$; *: $P < 0.05$; student's t-test).

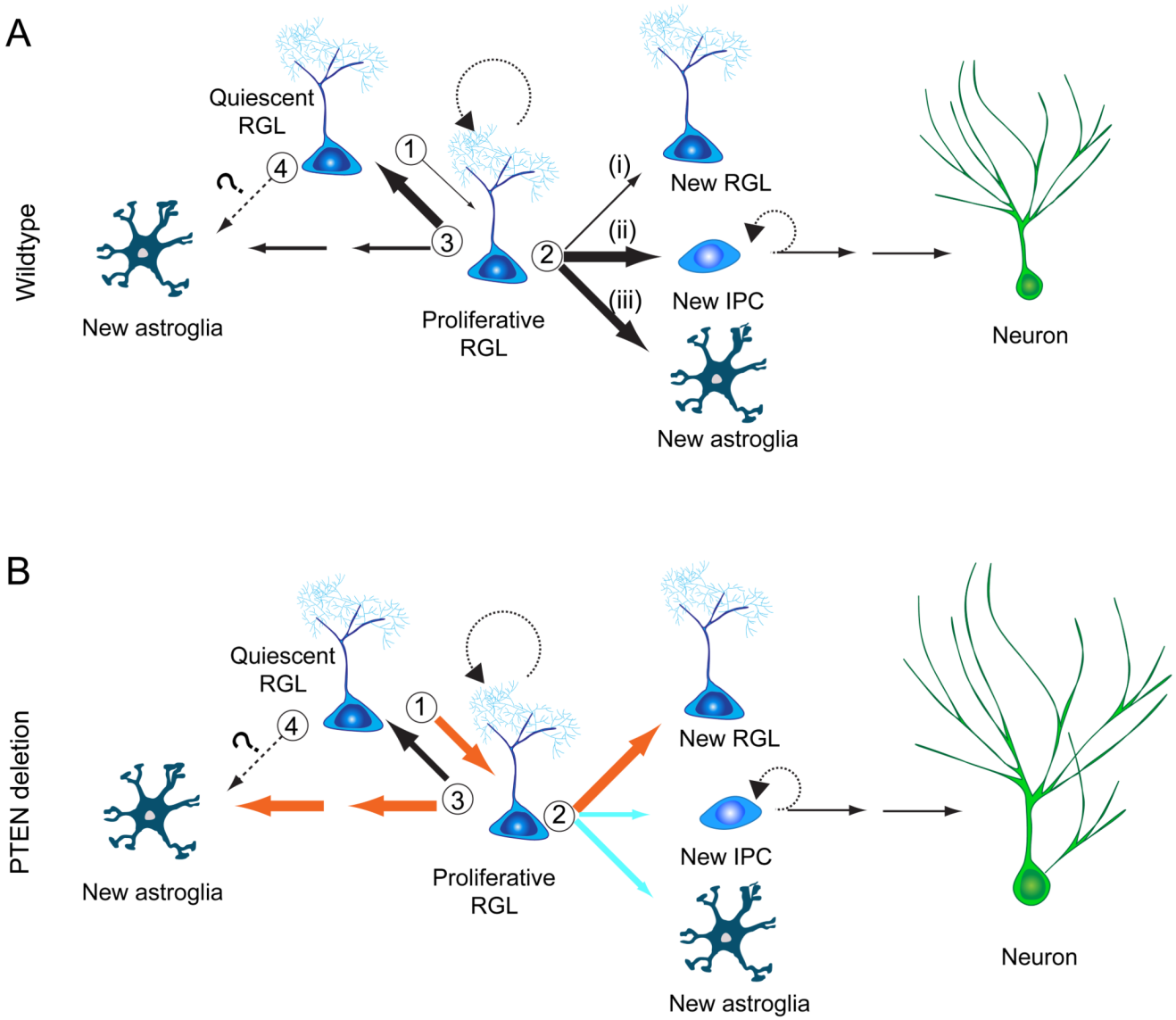

Figure 7. Models of nestin^{+} radial glia-like neural stem cell behavior in the adult hippocampus under basal conditions and after *Pten* deletion

(A) A model of the lineage relationship of RGLs in the young adult mouse hippocampus under basal conditions. There are at least three critical choice points: (1) An RGL decides to remain in quiescence or to become activated and enter the cell cycle; (2) An activated RGL can undergo one of three modes of self-renewal: (i) symmetric self-renewal to expand the RGL pool; (ii) neurogenic or (iii) astrogliogenic asymmetric self-renewal to generate a differentiated progeny while maintaining the RGL pool; (3) The RGL makes a choice between returning to quiescence and maintaining stemness or differentiating into an astrocyte via transition astroglia. (4) It is also possible that a quiescent RGL can directly differentiate into an astrocyte without cell division. The thickness of the arrow indicates the relative probability of each choice.

(B) A model on the role of PTEN in regulating RGLs in the young adult mouse hippocampus. *Pten* deletion in an RGL rapidly mobilizes it into cell cycle and fosters symmetric self-renewal. Over the long-term, PTEN loss promotes terminal differentiation of RGLs into astrocytes. PTEN loss in newborn neurons also leads to increased soma size and

dendritic complexity. Orange and blue arrows indicate increased and decreased probability, respectively.